International Journal of Heat and Mass Transfer 157 (2020) 119862

Contents lists available at ScienceDirect

International Journal of Heat and Mass Transfer

journal homepage: www.elsevier.com/locate/hmt

Topology optimization of time-transient heat conduction for thermo-optic silicon modulators

Gil Ho Yoon[a], Ercan M. Dede[b,*], Tsuyoshi Nomura[b,c], Paul Schmalenberg[b]

[a] School of Mechanical Engineering, Hanyang University, Seoul, South Korea
[b] Toyota Research Institute of North America, 1555 Woodridge Avenue, Ann Arbor, Michigan, 48105, USA
[c] Toyota Central R&D Labs., Inc., 41-1 Yokomichi, Nagakute, Aichi, 480–1192, Japan

ARTICLE INFO

Article history:
Received 25 September 2019
Revised 10 April 2020
Accepted 24 April 2020
Available online 18 June 2020

Keywords:
Thermo-optic effect
Transient analysis
Topology optimization

ABSTRACT

An optimization method is presented to enhance the time-transient thermal response of a thermo-optic silicon modulator. For the development of efficient opto-electronic devices, fast thermal response in a compact form factor is crucial to increasing modulator performance. Thus, to improve response, the layout of the modulator device is modified and tailored by structural topology optimization. The optimization approach considers the transient thermal response of the device with an adjoint sensitivity analysis of the transient system. A detailed design example for a silicon waveguide with an over-clad metal heater is provided, and results highlight a faster modulator temperature rise response with reduced out-of-plane length. The method is broadly applicable to a range of thermo-optic devices involving waveguides for next-generation sensors.

1. Introduction

Science and engineering approaches to controlling light-matter interactions in electromagnetic environments at nano and micro scales are being actively explored [1]. Understanding these interactions is of fundamental importance to applications ranging from optical sensing to communication and quantum science. In this context, silicon (Si) modulators are critical components in future nano-scale photonics devices [1]. In particular, the quick (on the order of microseconds) time-transient thermal response of Si modulators enables fast switching speed for next-generation optical communication devices and sensors. For example, Fig. 1 depicts an enlarged illustration of a representative photonics-based sensor.

Incoming laser light is coupled to nano-scale Si waveguides (or Si wires) to provide an electromagnetic wave that travels through laser splitters to Si modulators (i.e., phase shifters) that shift the phase of the light wave allowing for manipulation of the outgoing laser beam at an antenna array. The speed with which the phase shifters operate is critical to sensor performance. Additionally, while a single Si modulator might only consume a few milliwatts of power over a very small footprint area, the aggregation of hundreds of phase shifters into a physically larger sensor array drives up power consumption and affects the total parasitic loss of the device. This may lead to higher power densities for solid-state devices like the one shown in Fig. 1, which are typically on the millimeter scale and realized using state-of-the-art microfabrication techniques.

The shifting of the phase of the light wave in a Si modulator is generally achieved by exploiting the thermo-optic effect, where the refractive index inside a waveguide varies with the change in temperature of the material. Among various materials, Si shows a large thermo-optic effect, $\partial n/\partial T = 1.86 \times 10^{-4}$ (1/K) at 1.5 μm and 295 K, where the refraction index is n. The thermo-optic devices considered here are similar to prior devices studied in the literature [2], and the optical wavelength is similar. A common approach to enabling this effect is to use an over-clad metal heater [2] to impart a temperature change to the Si waveguide. However, as explained in the relevant research [3,4], such over-clad heaters may have a relatively slow thermal time constant due to a large thermal capacitance and thermal spreading that occurs during their use. Indeed, resistive effects in thermo-optic devices play an important role in the control of heat plus light, but these effects also reduce the efficiency of the modulator by dissipating power via the resistances. Thus, additional opportunities to optimize transient thermal response of thermo-optic devices and reduce parasitic power in a compact footprint exist, and some strategies [4–7] are to additionally etch surrounding Si or SiO_2 materials to effectively manipulate the device heat flow, time-transient behavior, and/or waveguide transmission characteristics. In the present work, this basic concept is extended further through de-

* Corresponding author.
E-mail address: eric.dede@toyota.com (E.M. Dede).

https://doi.org/10.1016/j.ijheatmasstransfer.2020.119862
0017-9310/

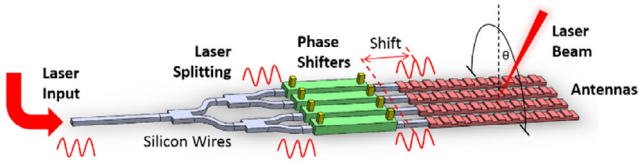

Fig. 1. Representative opto-electronic device.

tailed optimization of the SiO_2 insulating structure surrounding the waveguide.

Structural optimization schemes have helped to enhance device performance based on mathematical theory and numerical techniques. In particular, structural topology optimization allows one to explore optimal layouts without a prior given initial design and has been widely used in multiphysics system design [8,9]. Related to photonics, work exists on the topology optimization of splitters [10], waveguides [11], demultiplexers [12], and grating couplers [13,14], although the consideration of time-transient thermal response is generally neglected. Regarding heat transfer, relevant research has focused on shape or topology optimization for steady-state heat conduction [15,16]. Zhuang and Xiong proposed topology optimization for transient heat transfer minimizing the peak heat compliance and using transient sensitivity analysis [17]. To overcome difficulties, they further proposed the equivalent static load approach for the transient heat transfer problem. Evolutionary structural optimization, involving the removal and introduction of materials considering their contributions to the objective function, has been applied to the heat conduction problem [18–20]. Also, the level-set method with shape sensitivity analysis can be found [21,22] for topology optimization of steady-state heat conduction.

Despite the prolific work related to steady-state heat conduction, many heat conduction problems are transient in nature. It is therefore obvious and important for topology optimization to consider transient heat conduction. Yet, research in this field essentially demands transient analysis and related sensitivity analysis, both of which are not trivial. First-order sensitivity analysis of the transient heat conduction problem and its application to shape optimization are found in the literature [17,23–25]. Sensitivity analysis and shape optimization are additionally found in prior work [26–29]. Turteltaub used the temperature difference instead of heat compliance as the objective function in the context of transient heat conduction optimization [28]. An accurate time integration method for the sensitivity analysis of linear and nonlinear transient heat conduction problems was also proposed [29]. Compliant mechanism problems considering transient temperature response were further considered [30]. For topology optimization of a transient heat conduction problem, Zhuang et al. proposed a level set based topology optimization approach with the integral of the temperature gradient over a fixed time interval as an objective function [31]. Wu et al. [32] recently applied topology optimization to minimize the maximum temperature of transient heat conduction structures. Additionally, a variety of conjugate heat transfer interaction models have been investigated [33–35].

In this research, a topology optimization framework is developed considering the response of a transient heat transfer system, and it is applied to the performance enhancement of nano-scale waveguide structures for photonics-based applications. Specifically, a faster temperature rise response for a Si modulator with overclad metal heater is demonstrated, and it is further shown how the results lead to more compact modulator designs.

The paper is organized as follows. Section 2 provides background to the optimization of the time-transient response of thermo-optic devices, describes the governing equations for time-transient topology optimization under heat conduction, and presents the optical analysis method for performance evaluation. In Section 3, transient heat conduction optimization studies are considered, and Si modulator examples considering time-transient thermo-optic response are presented. Section 4 provides conclusions.

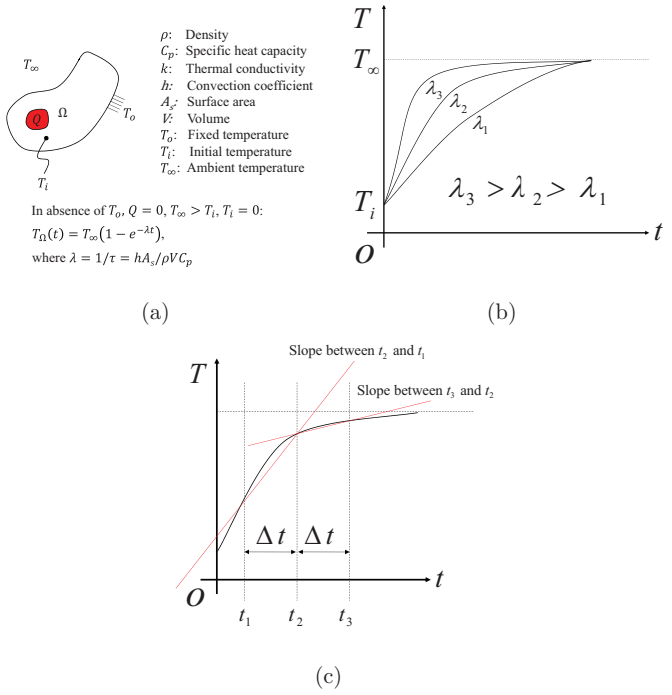

Fig. 2. (a) Transient heat conduction in a solid body assuming zero convective losses, (b) thermodynamic response for different λ, and (c) the physical meaning of the objective function.

2. Thermal-optics and topology optimization

In this section, the governing equations for a transient heat transfer system are introduced. This is followed by the detailed topology optimization formulation and the sensitivity analysis. Additional details are then provided on phase modulation in thermo-optic devices and an associated optical analysis in relation to time-transient thermal response.

2.1. Governing equations for transient heat transfer system

For the temperature field, T, the governing equation for the transient heat conduction problem, Fig. 2(a), can be formulated as follows:

$$\rho C_p \frac{\partial T}{\partial t} - k\nabla^2 T = Q, \quad t \in [0, t_f] \tag{1}$$

$$T|_{t=0} = T_i, \tag{2}$$

$$T = T_o \quad \text{on } \Gamma_D, \tag{3}$$

$$-k\frac{\partial T}{\partial n_N} = q'' \quad \text{on } \Gamma_N, \tag{4}$$

$$-k\frac{\partial T}{\partial n_C} = q''_h = h(T - T_\infty) \quad \text{on } \Gamma_C, \tag{5}$$

where the material density, the specific heat capacitance, and the thermal conductivity are denoted by ρ, C_p, and k, respectively. The

rate of the internal heat generation is Q, and the terminal time is t_f. The initial temperature, the prescribed temperature on Γ_D, and the heat flux on Γ_N are denoted by T_i, T_o, and q'', respectively. The normal direction to boundaries Γ_N and Γ_C are denoted, respectively, by n_N and n_C. The convective heat flux, q''_h, boundary condition on Γ_C is defined by the convection coefficient, h, and the ambient temperature, T_∞. Here, we assume zero radiative losses, and thus an equivalent lumped capacitance problem is as shown in Fig. 2(a).

Applying the finite element method (FEM), solutions to the transient heat transfer equation are governed by a system of first order linear differential equations:

$$\mathbf{C}\dot{\mathbf{T}} + \mathbf{K}\mathbf{T} = \mathbf{Q}, \quad \mathbf{T}|_{t=0} = \mathbf{T}_i, \quad t \in [0, t_f], \tag{6}$$

where the global heat capacity matrix and the global stiffness/conductivity matrix are denoted by $\mathbf{C}$ and $\mathbf{K}$, respectively. The temperature derivatives with respect to time and the nodal temperatures are, respectively, denoted by $\dot{\mathbf{T}}$ and $\mathbf{T}$. The initial temperature distribution vector is denoted by $\mathbf{T}_i$.

2.2. Topology optimization formulation for thermo-optic application

Using thermodynamic theory, simplified by a lumped parameter model with the assumption of a uniform temperature inside an objective domain and a sufficiently small Biot number, the differences among integrals can be used to extract the exponent of the response. Specifically, to find the coefficient, λ, governing the transient system response, the integrals of the temperature (T_1, T_2 and T_3) of the waveguide domain at three distinct times, i.e., at t_1, t_2 and t_3, with a consistent time interval are computed and combined as written in (7) and shown in Figs. 2(b) and (c).

$$T_2 - T_1 = \int_\Omega e^{-\lambda t_2}(T_i - T_\infty) - e^{-\lambda t_1}(T_i - T_\infty)dx \tag{7}$$

$$T_3 - T_2 = \int_\Omega e^{-\lambda t_3}(T_i - T_\infty) - e^{-\lambda t_2}(T_i - T_\infty)dx$$

$$\begin{aligned}\frac{T_3 - T_2}{T_2 - T_1} &= \frac{\int_\Omega e^{-\lambda t_3} - e^{-\lambda t_2}dx}{\int_\Omega e^{-\lambda t_2} - e^{-\lambda t_1}dx} \\ &= \frac{\int_\Omega e^{-\lambda(t_1+2\Delta t)} - e^{-\lambda(t_1+\Delta t)}dx}{\int_\Omega e^{-\lambda(t_1+\Delta t)} - e^{-\lambda t_1}dx} \\ &= \int_\Omega e^{-\lambda \Delta t}dx\end{aligned}$$

$$\log\left(\frac{T_3 - T_2}{T_2 - T_1}\right) = -\int_\Omega \lambda \Delta t dx,$$

$$\lambda = \frac{1}{\Delta t \int_\Omega dx}\log\left(\frac{T_2 - T_1}{T_3 - T_2}\right)$$

The above equations illustrate that the temperature of the thermodynamic system increases exponentially from its initial temperature value to a steady state value.

In order to maximize λ, it is alternatively possible to maximize the function, $(T_2 - T_1)/(T_3 - T_2)$. Therefore, the following optimization formulation in (8) is used in the present study to find optimal layouts for thermo-optic application.

$$\begin{aligned}&\underset{\gamma}{\text{Max}} \quad \Phi = \tfrac{T_2 - T_1}{T_3 - T_2} \\ &\text{Subject to mass constraint}\end{aligned} \tag{8}$$

Physically, the objective function in (8) can be interpreted as the minimization of the thermal time constant, τ, for an ambient temperature of the system since $\lambda = 1/\tau$. Here, the objective function, Φ, is related to the coefficient, λ, of the transient thermodynamic system with the design variable, γ, defined at each finite element, and a mass constraint.

For the topology optimization, the material properties should be interpolated with respect to the design variables assigned to each finite element. Solid isotropic material with penalization (SIMP) based interpolations are employed. The interpolation equations are formulated as follows:

$$C_p = C_{\text{nominal}} \times \gamma^{p_1}, \quad k = k_{\text{nominal}} \times \gamma^{p_2} \tag{9}$$

$$\gamma = \epsilon : \text{Void}, \quad \gamma = 1 : \text{SiO}_2, \tag{10}$$

where the SIMP penalization factors of C_p and k with respect to the design variable are p_1 and p_2, respectively. Depending on the values of the penalization factors, different local optimal solutions are obtained. These values are set between 4 to 6 for all examples. In order to avoid singularity of the FEM solution, a very small value is assigned for $\gamma_{\min}$, i.e., $\epsilon = 0.001$. It is found that the energy stored in finite elements having low density is sufficiently small and can be neglected; imaginary temperatures of the void region in this problem are analogous to imaginary structural displacements of the void region in a compliance minimization topology optimization problem. The material density, ρ in (1), is not interpolated, as the heat capacitance, C_p, is multiplied with the mass density.

Thus, a topology optimization formulation for a general transient heat transfer problem can be stated as follows:

$$\begin{aligned}&\underset{\gamma}{\text{Min}} \int_0^{t_f} f(\mathbf{T}, \gamma)dt \\ &\text{Subject to } g_i \leqslant 0, \quad i = 1, 2, \ldots, N_c \\ &\gamma = [\gamma_1, \gamma_2, \ldots, \gamma_{N_e}], \quad \epsilon \leqslant \gamma \leqslant 1\end{aligned} \tag{11}$$

where the objective function and constraints are denoted by f and g_i, respectively. Without loss of generality, the objective function is set as the integral of a function of the temperature and the design variable. The number of constraints is N_c, and the number of design variables, $\boldsymbol{\gamma}$, is N_e.

To derive the sensitivity values of the objective function with respect to the design variables, the Lagrangian combining the objective function and the time integral of the governing equation with the Lagrange multiplier, $\boldsymbol{\lambda_t}$, is formulated. The sensitivity analysis of the transient system can be found in the literature [36]. For completeness, the derivations are included here.

$$\begin{aligned}L = &\int_0^{t_f} f(\mathbf{T}, \gamma)dt + \int_0^{t_f} \boldsymbol{\lambda_t}^{\mathrm{T}}\left[\mathbf{C}\dot{\mathbf{T}} + \mathbf{K}\mathbf{T} - \mathbf{Q}\right]dt \\ &(\mathbf{T}|_{t=0} = \mathbf{T}_i, t \in [0, \quad t_f])\end{aligned} \tag{12}$$

where the derivative of L with respect to the e-th design variable, γ_e, can be summarized as follows:

$$\begin{aligned}\frac{\partial L}{\partial \gamma_e} &= \int_0^{t_f} \frac{\partial f}{\partial \gamma_e} + \frac{\partial f}{\partial \mathbf{T}}\frac{\partial \mathbf{T}}{\partial \gamma_e}dt \\ &\quad + \frac{\partial}{\partial \gamma_e}\left(\int_0^{t_f} \boldsymbol{\lambda_t}^{\mathrm{T}}\left[\mathbf{C}\dot{\mathbf{T}} + \mathbf{K}\mathbf{T} - \mathbf{Q}\right]dt\right) \\ &= \int_0^{t_f} \frac{\partial f}{\partial \gamma_e} + \frac{\partial f}{\partial \mathbf{T}}\frac{\partial \mathbf{T}}{\partial \gamma_e}dt \\ &\quad + \int_0^{t_f} \boldsymbol{\lambda_t}^{\mathrm{T}}\left[\frac{\partial \mathbf{C}}{\partial \gamma_e}\dot{\mathbf{T}} + \mathbf{C}\frac{\partial \dot{\mathbf{T}}}{\partial \gamma_e} + \frac{\partial \mathbf{K}}{\partial \gamma_e}\mathbf{T} + \mathbf{K}\frac{\partial \mathbf{T}}{\partial \gamma_e} - \frac{\partial \mathbf{Q}}{\partial \gamma_e}\right]dt \\ &\quad \text{with } \frac{\partial \mathbf{Q}}{\partial \gamma_e} = \mathbf{0} \\ &= \int_0^{t_f} \frac{\partial f}{\partial \gamma_e} + \frac{\partial f}{\partial \mathbf{T}}\frac{\partial \mathbf{T}}{\partial \gamma_e}dt \\ &\quad + \int_0^{t_f} \boldsymbol{\lambda_t}^{\mathrm{T}}\left[\frac{\partial \mathbf{C}}{\partial \gamma_e}\dot{\mathbf{T}} + \mathbf{C}\frac{\partial \dot{\mathbf{T}}}{\partial \gamma_e} + \frac{\partial \mathbf{K}}{\partial \gamma_e}\mathbf{T} + \mathbf{K}\frac{\partial \mathbf{T}}{\partial \gamma_e}\right]dt\end{aligned} \tag{13}$$

In order to derive the term $\int_0^{t_f} \lambda_t{}^T \mathbf{C} \frac{d\dot{\mathbf{T}}}{d\gamma_e} dt$, the following are formulated.

$$\int_0^{t_f} \frac{d}{dt}\left(\lambda_t{}^T \mathbf{C} \frac{\partial \mathbf{T}}{\partial \gamma_e}\right) dt = \int_0^{t_f} \left(\frac{d}{dt}\left(\lambda_t{}^T \mathbf{C}\right) \frac{\partial \mathbf{T}}{\partial \gamma_e} + \lambda_t{}^T \mathbf{C} \frac{d\dot{\mathbf{T}}}{d\gamma_e}\right) dt$$
$$= \lambda_t{}^T \mathbf{C} \frac{\partial \mathbf{T}}{\partial \gamma_e}\Big|_0^{t_f} \tag{14}$$

$$\int_0^{t_f} \lambda_t{}^T \mathbf{C} \frac{d\dot{\mathbf{T}}}{d\gamma_e} dt = \lambda_t{}^T \mathbf{C} \frac{\partial \mathbf{T}}{\partial \gamma_e}\Big|_0^{t_f} - \int_0^{t_f} \frac{d}{dt}\left(\lambda_t{}^T \mathbf{C}\right) \frac{\partial \mathbf{T}}{\partial \gamma_e} dt \tag{15}$$

By inserting the above results into (13), the final transient sensitivity of the objective function can be written as:

$$\frac{\partial L}{\partial \gamma_e} = \int_0^{t_f} \frac{\partial f}{\partial \gamma_e} + \frac{\partial f}{\partial \mathbf{T}} \frac{\partial \mathbf{T}}{\partial \gamma_e} dt$$
$$+ \int_0^{t_f} \lambda_t{}^T \left[\frac{\partial \mathbf{C}}{\partial \gamma_e}\dot{\mathbf{T}} + \frac{\partial \mathbf{K}}{\partial \gamma_e}\mathbf{T} + \mathbf{K}\frac{\partial \mathbf{T}}{\partial \gamma_e}\right] dt$$
$$+ \lambda_t{}^T \mathbf{C} \frac{\partial \mathbf{T}}{\partial \gamma_e}\Big|_0^{t_f} - \int_0^{t_f} \frac{d}{dt}\left(\lambda_t{}^T \mathbf{C}\right) \frac{\partial \mathbf{T}}{\partial \gamma_e} dt$$
$$= \int_0^{t_f} \frac{\partial f}{\partial \gamma_e} + \lambda_t{}^T \left[\frac{\partial \mathbf{C}}{\partial \gamma_e}\dot{\mathbf{T}} + \frac{\partial \mathbf{K}}{\partial \gamma_e}\mathbf{T}\right] dt \tag{16}$$

It is assumed that the thermal loads and initial conditions are independent of the design variables, that is $\frac{\partial \mathbf{Q}}{\partial \gamma_e} = \mathbf{0}$ and $\frac{\partial \mathbf{T}}{\partial \gamma_e}\Big|_{t=0} = \mathbf{0}$. The Lagrangian multiplier is then computed by solving the following adjoint system.

$$-\mathbf{C}\dot{\lambda}_t + \lambda_t{}^T \mathbf{K} = -\frac{\partial f}{\partial \mathbf{T}}, \quad t \in [0, t_f]$$
$$\lambda_t(t_f) = \mathbf{0}, \quad \dot{\lambda}_t(t_f) = \mathbf{0} \tag{17}$$

Since the above equation is a final value problem, a time reversal FEM is employed to solve it.

2.3. Phase modulation in thermo-optic devices

Phase modulation in thermo-optic nano-waveguide devices is achieved through controlled changes of the refractive index, n, of the material comprising the waveguides. The magnitude of the relative phase change is determined by the magnitude of the refractive index change and the length along the waveguide where the refractive index change is affected. Typically, it is desirable to minimize the size of phase modulation devices so that the change in the refractive index should be maximized. For most applications, the relative phase shift between the base state and fully tuned state should be at least 2π.

One method to inflict the refractive index change is to tune the temperature of the material. In most materials, this change in n is the result of density decreasing with an increased temperature. With Si, the change is magnified due to the contribution of bound electrons in the semiconductor's crystalline lattice. Many properties of the Si making up the waveguides, such as dopants or lattice defects, influence the exact variation in n with respect to temperature, so that $\partial n/\partial T$ is found empirically by various measurement techniques and is generally linear at room temperature, e.g. ~ 293 K, and above.

To create a small device, the temperature tuning range or change in temperature, ΔT, is chosen to be a few hundred degrees. The drawback of this approach, and relatively large required ΔT, is that the time constant between the base state and fully tuned state is large, which is in direct conflict with realizing a fast modulator. As such, there is a need for new techniques to optimize the speed, and hence thermal response, of compact Si modulators.

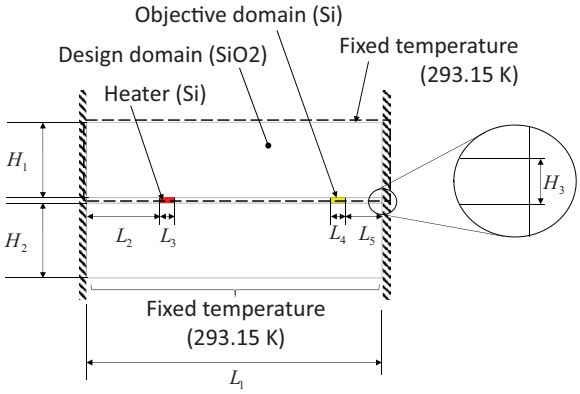

Fig. 3. Example design domain. Heat source: 10 mW for 10 μs; SiO_2 properties: $C_p = 703$ J/kg × K, $\rho = 2203$ kg/m^3, $k = 1.38$ W/m × K; Si properties: $C_p = 700$ J/kg × K, $\rho = 2329$ kg/m^3, $k = 130$ W/m × K; Structure dimensions: $L_1 = 12$ μm, $L_2 = 3$ μm, $L_3 = 0.6$ μm, $L_4 = 0.6$ μm, $L_5 = 1.4$ μm, $H_1 = 3$ μm, $H_2 = 3$ μm, $H_3 = 0.22$ μm.

To find the difference in the speed of propagation between cold and heated Si modulator states, boundary mode analysis is performed once the heat transfer analysis is completed to solve for the propagation constant at each simulated thermal step. FEM is utilized to find the modes by solving reduced electromagnetic vector-wave equations [37] of the form:

$$\nabla_{tr}^2 \mathbf{E}_{tr} + (k_o^2 \varepsilon - \beta^2)\mathbf{E}_{tr} = -\nabla\left(\mathbf{E}_{tr} \cdot \frac{\nabla_{tr}\varepsilon}{\varepsilon}\right), \tag{18}$$

where all subscripts, tr, refer to transverse waves (in this case in x and y in-plane directions for two-dimensional (2-D) waveguide cross-sections considered here), ε is material permittivity which is a function of defined material and simulated temperature, β is the propagation constant, and k_o is the wave number. This reduced form is achieved by setting permeability in all situations to unity. While this equation is in terms of the electric field, **E**, typically it is recast in terms of the magnetic field in practice.

With β found via (18) for all time steps, the average of the gradient for both the heating and cooling times of a Si modulator thermal cycle are taken as,

$$A = \frac{1}{n_{tm}} \sum_0^{n_{tm}} \frac{\beta_{i+\Delta t_m} - \beta_i}{\Delta t_m}. \tag{19}$$

In the analysis here, the time period from 0 to t_m is defined as the same period for 200 kHz or 5 μs. The time step, Δt_m, and number of time steps, n_{tm}, is the same as that used for the preceding heat transfer physics. After both the averages of the heating and cooling changes in the propagation constant are found, the absolute value of both are averaged together so that performance over a full thermal cycle is taken into account.

With (19), which is in units of radians per micrometer per microsecond, the required out-of-plane waveguide length, in microns, of a 200 kHz (typical value) Si modulator to reach 2π phase shift is found as,

$$l = \frac{2\pi}{A \cdot 5}. \tag{20}$$

3. Numerical studies

To validate the concept of applying topology optimization to thermo-optic design, this section provides optimal layouts for Si modulator related devices considering time-transient thermal response as an objective function. 2-D layouts are first considered to present fundamental concepts related to these devices, the optimized results, and the improved performance of the designs. In

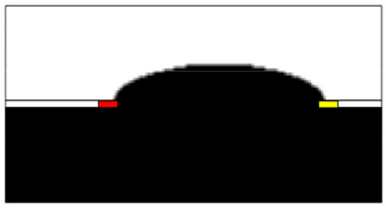

(a)

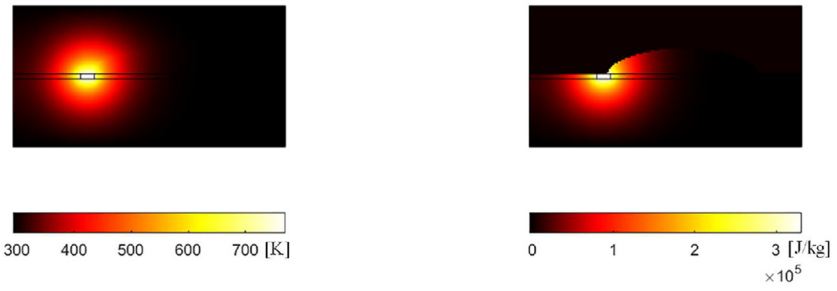

(b)

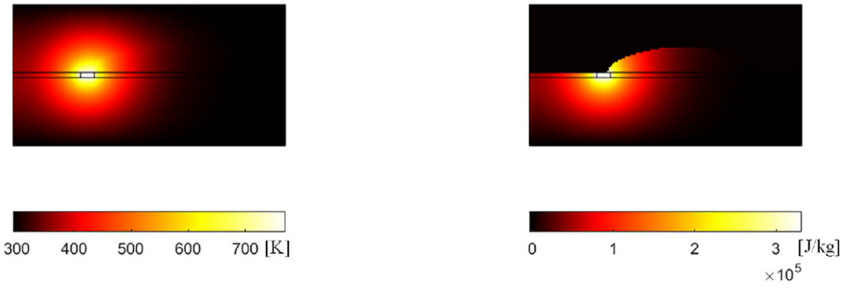

(c)

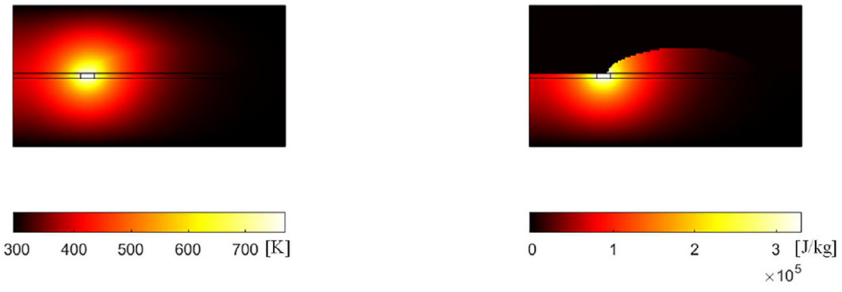

(d)

Fig. 4. Benchmark example results: (a) optimized layout with mass = 15.84% (note: dark regions in design domain = SiO_2, light regions = void); temperature, left column, and internal energy per unit mass, right column, at (b) 2 μs, (c) 4 μs, and (d) 6 μs.

order to solve the optimization problem, the method of moving asymptotes (MMA) algorithm [38] in a custom-scripted computing environment [39] is employed. A three-dimensional (3-D) example is then provided as a logical extension of the 2-D work.

3.1. Benchmark 2-D example problem

As a benchmark first example, Fig. 3, an optimization problem maximizing a specified domain temperature subject to a mass constraint,

$$\begin{aligned} &\underset{\gamma}{\text{Max}} \int_{\Omega_o} T dx \Big|_{t=6\mu s} \\ &\text{Subject to mass} \leqslant 50\% \\ &\gamma = [\gamma_1, \gamma_2, \ldots, \gamma_{N_e}], \quad \gamma_{\min} \leqslant \gamma \leqslant 1 \end{aligned} \tag{21}$$

is considered on a 2-D structure cross-section. A heater is embedded in a SiO_2 substrate, and it is assumed that a Si waveguide structure is installed near the right-side center of the domain.

Rather than considering the exponent of the response curve as an objective function, the maximization of the temperature in the objective domain, Ω_o, is considered for this problem to verify the expected behavior of the developed optimization framework for the transient system as opposed to a steady-state conduction system. The design domain is made of SiO_2, while the heater and the waveguide (objective domain) are made of Si. An adiabatic condition is imposed along the left and right boundaries, and a fixed temperature, 293.15 K, is imposed at the top and bottom surfaces of the domain.

The objective function is evaluated as the integral of the temperature inside the waveguide domain at 6 μs. The semi-ellipse shaped optimal design in Fig. 4 with 15.84% mass is obtained. It is interesting that the ends of the semi-ellipse are partially connecting the heater and the waveguide. Only considering thermal conduction, it is better to connect the heater and the waveguide using the entire SiO_2 top-side material, but due to the effect of the thermal capacitance, the optimizer alternatively finds the semi-ellipse shaped design with 15.84% mass fraction. Note that with this material property, the solution times are not sufficient to reach a steady-state solution. Fig. 4(b), (c) and (d) show the domain temperature and the internal energy per unit mass in the left and right columns at 2 μs, 4 μs, and 6 μs, respectively. It appears that the thermal energy is progressively transferred toward the waveguide, and the energy per unit mass of the void region becomes zero indicating that the present material interpolation scheme is successful in topologically optimizing solid and void domains.

To further test the effect of material properties on the design, Fig. 5 shows an optimal structure with the same conditions but with an artificially reduced (0.01% of its original value) thermal capacitance of the SiO_2 material. With this lower capacitance, a design covering the heater and the objective domain (with structural mass at the upper bound limit) is obtained due to the larger effect of the SiO_2 thermal conductance on the solution.

3.2. Design for thermo-optic response

For topology optimization of time-transient temperature response of a thermo-optic device, a Si waveguide buried in a SiO_2 layer with a metal over-clad heater is considered, as shown in Fig. 6(a).

Here, we consider a 2-D cross-section of this Si modulator, Fig. 6(b), with an out-of-plane (z-direction) depth of 100 μm; the representative in-plane dimensions are provided in Fig. 6(c). The Tungsten (W) heater power is 50 mW applied for 10 μs with a fixed temperature boundary condition, 293.15 K, applied at the bottom edge of the entire structure; adiabatic boundary conditions are imposed elsewhere. The waveguide is supported by a fixed

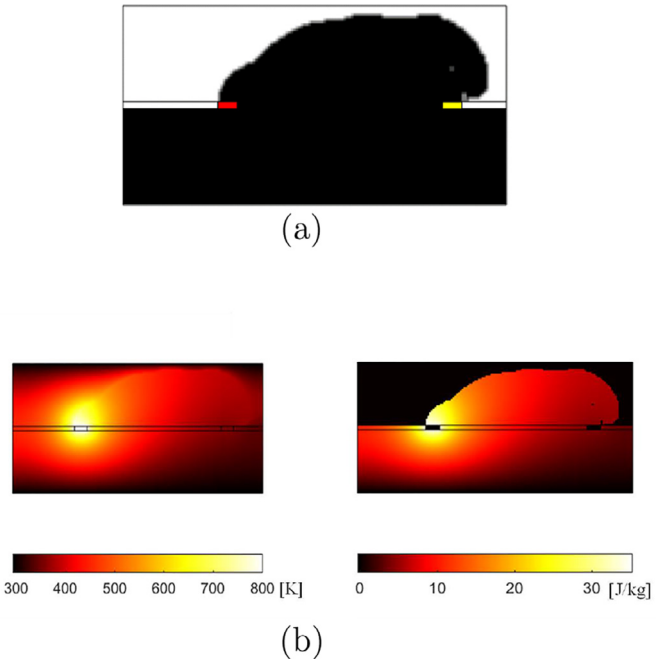

Fig. 5. Benchmark example results using a different lower capacitance for Si, (703E-4 J/kg × K): (a) optimized layout with mass = 50% (note: dark regions in design domain = SiO_2, light regions = void); (b) temperature, left column, and internal energy per unit mass, right column, at 6 μs.

SiO_2 pillar, as indicated in Fig. 6(b). The remaining SiO_2 material is then set as the design domain for topology optimization. In the optimization formulation, we utilize the exponent coefficient as an objective function with a mass constraint, per (8). To compute the objective function, the temperature inside the Si waveguide domain shown in Fig. 6(b) is integrated, and the derivatives with respect to time at 2 μs, 4 μs, and 6 μs are consecutively computed.

Fig. 7 shows the optimization results (with temperature contours at the 10 μs peak) for a range of mass constraint values including SiO_2 volume fractions of 95%, 90%, 80%, 70%, 60%, 45%, 30%, and 15%. Observe that at higher volume fraction values (e.g. 95%, 90%, 80%, 70%) the optimizer first seeks to decouple the support base of the SiO_2 material below the Si waveguide from the surrounding SiO_2 material in an effort to thermally isolate the waveguide. Then, at progressively lower volume fractions (e.g. 60%, 45%, 30%, 15%) the optimizer reduces the width of the support pillar effectively reducing the thermal capacitance of the waveguide support structure.

The transient thermal response over 20 μs (i.e. 10 μs of heating followed by 10 μs of cooling) for each different volume fraction design is provided in Fig. 8. In both heating and cooling regimes, steady-state response is not achieved, and this is typical for such devices. Further observe in Fig. 8 that, as the amount of SiO_2 material is reduced, the rate at which the Si modulator responds increases, and the maximum (non-steady-state) device temperature around 10 μs increases from 529 K for the 95% SiO_2 volume fraction case to 871 K for the 15% SiO_2 volume fraction design. This result confirms that greater etching around the base pedestal of the SiO_2 structure indeed provides faster temperature rise response.

Interestingly, the results in Fig. 7 are consistent with independent studies, [6], that have shown complete under-etching of suspended Si modulator structures are feasible and beneficial for enhanced thermo-optic response, although here the geometries are obtained automatically through the optimization procedure. We should further note that these results may serve as a conceptual guide, and for practical arrays of modulators, such as those needed to realize a large sensor as shown in Fig. 1, manufacturability and

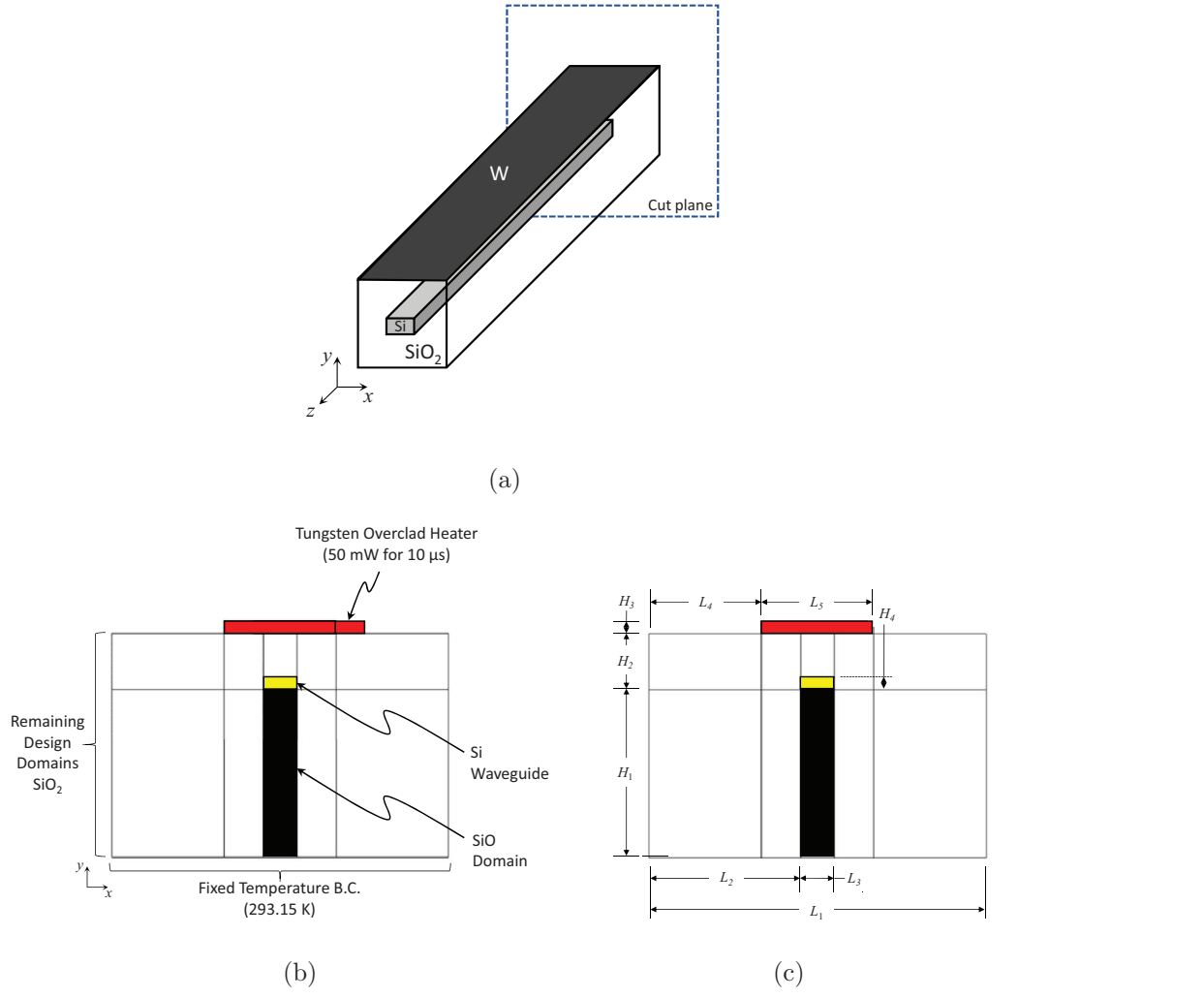

Fig. 6. (a) Si modulator embedded in SiO_2 with over-clad W metal strip heater. (b) Representative cross-section of Si modulator on an $x - y$ cut plane; heat source: 10 mW for 10 μs; SiO_2 properties: $C_p = 703$ J/kg × K, $\rho = 2203$ kg/m^3, $k = 1.38$ W/m × K; Si properties: $C_p = 700$ J/kg × K, $\rho = 2329$ kg/m^3, $k = 130$ W/m × K; W properties: C_p=132 J/kg × K, $\rho = 17800$ kg/m^3, $k = 175$ W/m × K. (c) Structure dimensions: $L_1 = 6$ μm, $L_2 = 2.7$ μm, $L_3 = 0.6$ μm, $L_4 = 2$ μm, $L_5 = 2$ μm, $H_1 = 3$ μm, $H_2 = 1$ μm, $H_3 = 0.22$ μm, $H_4 = 0.22$ μm.

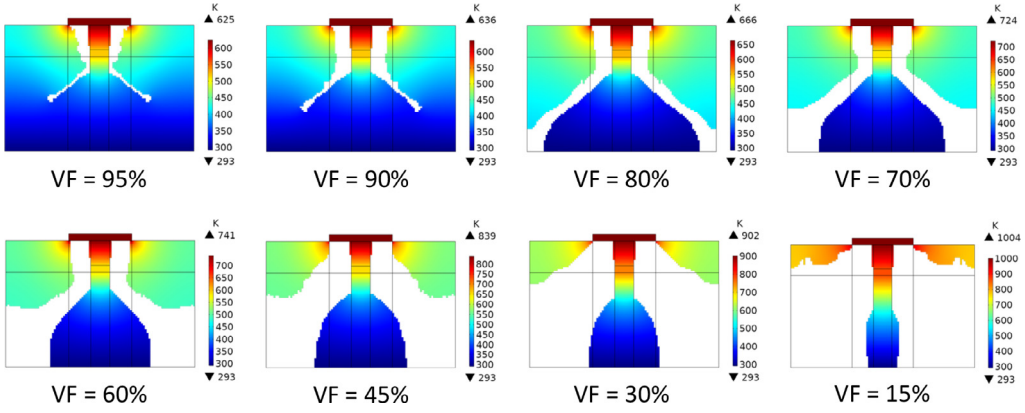

Fig. 7. Topology optimization results for different SiO_2 material volume fractions (VF) with temperature contours at the $t = 10$ μs peak. Note: light colored regions in design domain = void.

thermal cross-talk should be considered. Thus, implementation of a manufacturing constraint, as discussed in [9] is possible to realize designs that are compatible with commercial silicon photonics foundry processes. Alternatively, further post-processing is available, and as an example, the design for 15% volume fraction of SiO_2 is manually refined by removing the SiO_2 material directly to the left and right of the over-clad heater. From Fig. 7, we infer that this material is unnecessary for SiO_2 volume fractions less than 90%. Two modulators are then positioned side by side at a 0.5 μm spacing with a 3 μm thick Si layer below the modulators to represent the silicon-on-insulator (SOI) wafer handling layer; refer to the original and refined 2-D models in Fig. 9(a).

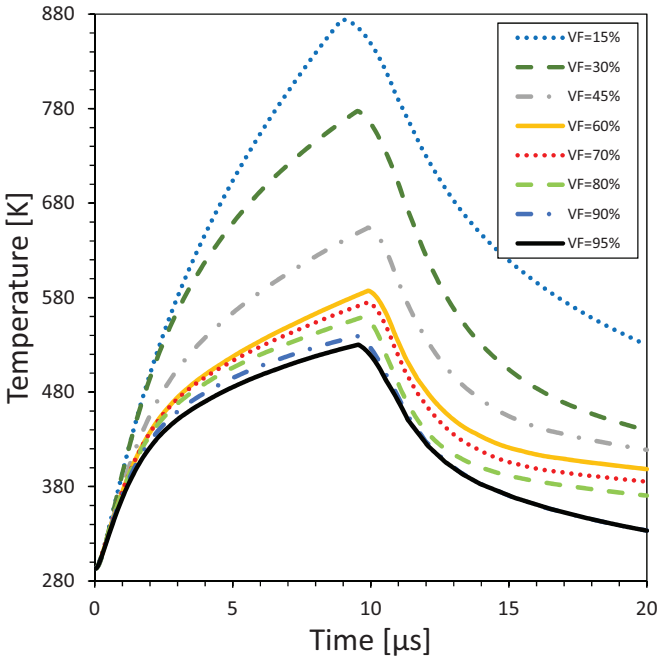

Fig. 8. Time-transient maximum temperature response of Si modulator waveguide for different SiO_2 material volume fractions (VF).

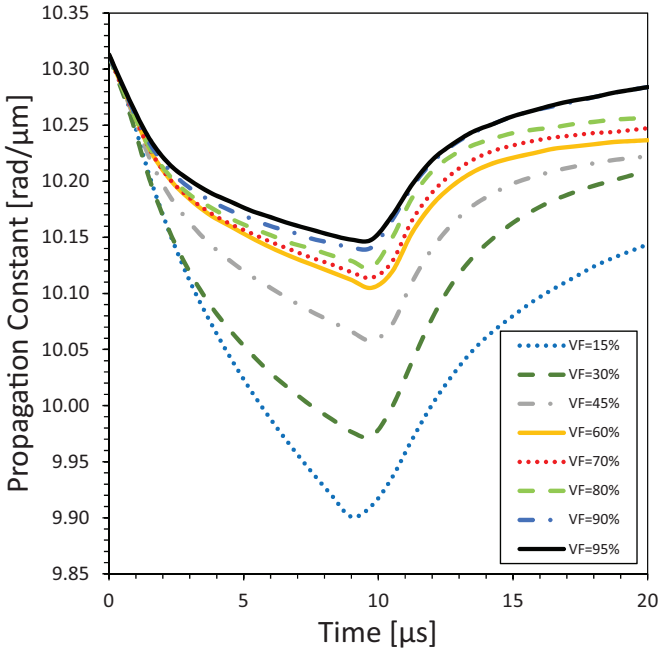

Fig. 10. Propagation constant of Si modulator waveguide for different SiO_2 material volume fractions (VF).

Such refined designs may be more amenable to existing SOI etching techniques [40] and exhibit minimal thermal cross-talk since modulator-to-modulator spacing (or pitch) is simply limited by the width of the base SiO_2 pillar supporting each waveguide; please note the different y-axis scales for the graphs in Fig. 9(b), which illustrate waveguide transient thermal response and minimal thermal cross-talk.

Regarding optical performance, the Si modulator response for each SiO_2 volume fraction design is computed following the procedure outlined in Section 2.3. The resulting propagation constant, β, for each design is shown in Fig. 10, and as the amount of SiO_2 material is reduced, the change in the propagation constant of the fundamental mode increases between the initial time and 10 μs indicating a faster change in the phase of the electromagnetic wave passing out-of-plane through the Si waveguide. This faster change

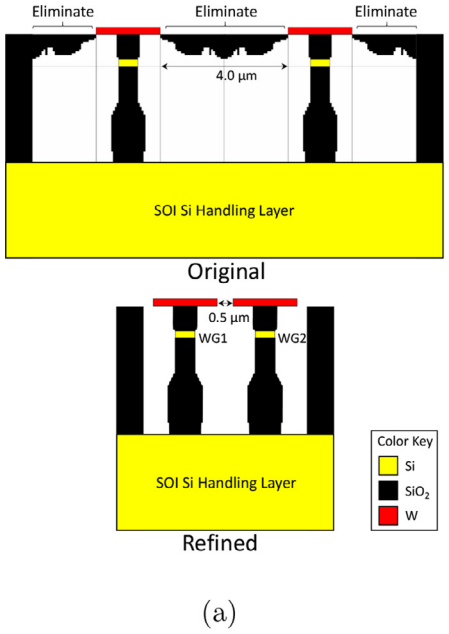

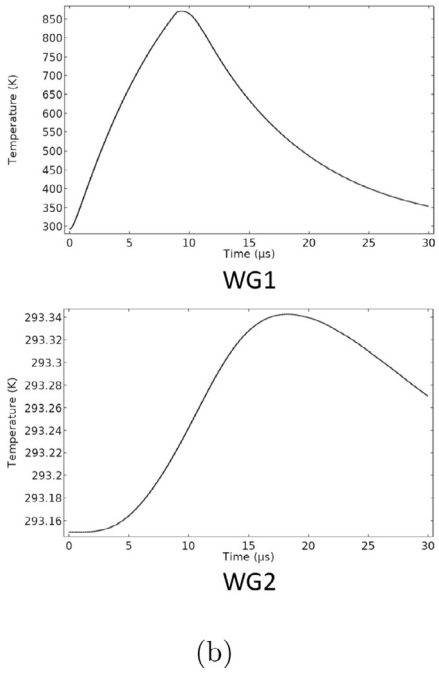

Fig. 9. (a) An array of two original 15% SiO_2 volume fraction design modulators, and a corresponding refined modulator array design for compact packaging and minimal thermal cross-talk. (b) Time-transient thermal response of Si waveguides 1 and 2, WG1 and WG2, respectively, over 30 μs with power applied to the W heater for WG1 for the first 10 μs. Note that the lowest boundary of the SOI Si handling layer is fixed to 293.15 K.

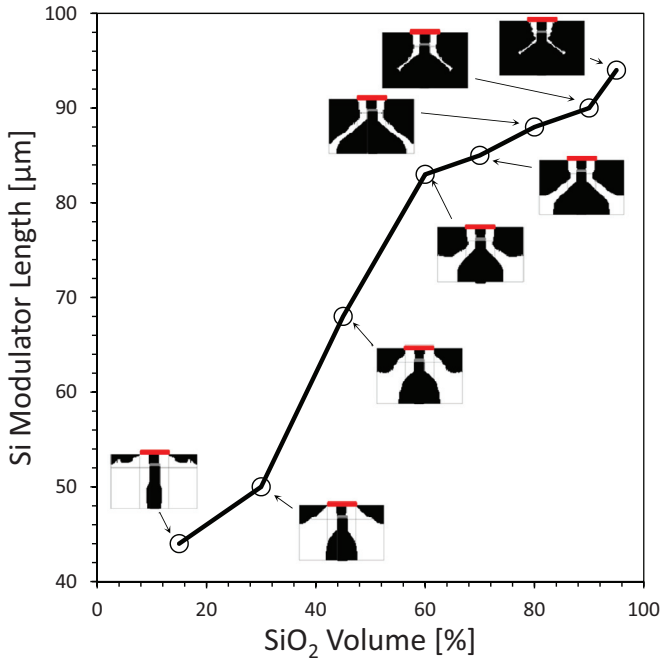

Fig. 11. Out-of-plane length of Si modulator waveguide for different SiO_2 material volume percentages.

of phase equates to a smaller device, as shown in Fig. 11, where the out-of-plane length of each Si modulator design is graphed based on the calculation in (20). Note that more substantial reductions in the Si modulator length are obtainable using lower volume fraction (60%, 45%, 30%, 15%) SiO_2 material designs. The voltage required to drive the heater is also length dependent and decreases with shorter lengths from 0.77 V to 0.53 V based on an analysis using the considered heater geometries and materials. Furthermore, while relatively simple modulator geometry is used in this study where the Si waveguide is positioned directly below the heater, the trend in Figs. 8–11 implies that modulators with different relative distances to a heat source, e.g. as shown in [41], may be further thermally and hence optically tuned by logically controlling the etching of the surrounding SiO_2 material in combination with spatially optimizing the modulator length for compactness.

From a thermo-optic perspective, the preceding results and discussion indicate that shorter optimized modulator designs are feasible to achieve a 2π phase shift. However, practical limitations may exist when considering specific heater geometries and materials in terms of reliability, electromigration, and mean time to failure (MTTF). As an alternative, longer modulators may still be employed while also utilizing an optimized modulator topology to balance enhanced performance with MTTF. For example, the 15% SiO_2 volume fraction design in Fig. 8 can achieve the same maximum temperature as the 95% SiO_2 volume fraction design (assuming the same length) in one-fifth the time. Thus, higher temperature is not required to achieve a 2π phase shift assuming the same modulator length, and faster response instead becomes the leading performance benefit.

3.3. Extension to 3-D

The above results may be further explored in the context of a 3-D optimization example for a similar Si modulator with over-clad heater to understand end effects not captured in two dimensions. In this case, the same modulator cross-section geometry, as shown in Fig. 6, is considered with an out-of-plane, z-direction, length of 10 μm; the relatively short length is selected here to minimize computational cost while being sufficient to visualize and gain insight into the structure end effects from the time transient optimization. A one-quarter symmetry model is shown in Fig. 12 on the left side, where the total z-direction depth of the model includes one-half of the modulator length (i.e. 5 μm) plus an additional 3 μm of waveguide end length.

A total heater power of 50 mW is again applied with a fixed, 293.15 K, temperature boundary condition at the lowest $x-z$ surface of the model. The optimization results for a SiO_2 volume fraction of 30% is shown on the right in Fig. 12. The result shows similar trends to the what was found in 2-D, where a pillar of SiO_2 directly connecting the heater and waveguide is retained and the remaining SiO_2 is positioned near to the fixed SiO_2 pedestal. In Fig. 12, the waveguide centerline temperature at $t = 0.5$ μs is superimposed on the optimization result as a line with y-direction height proportional to the temperature magnitude. Observe that at

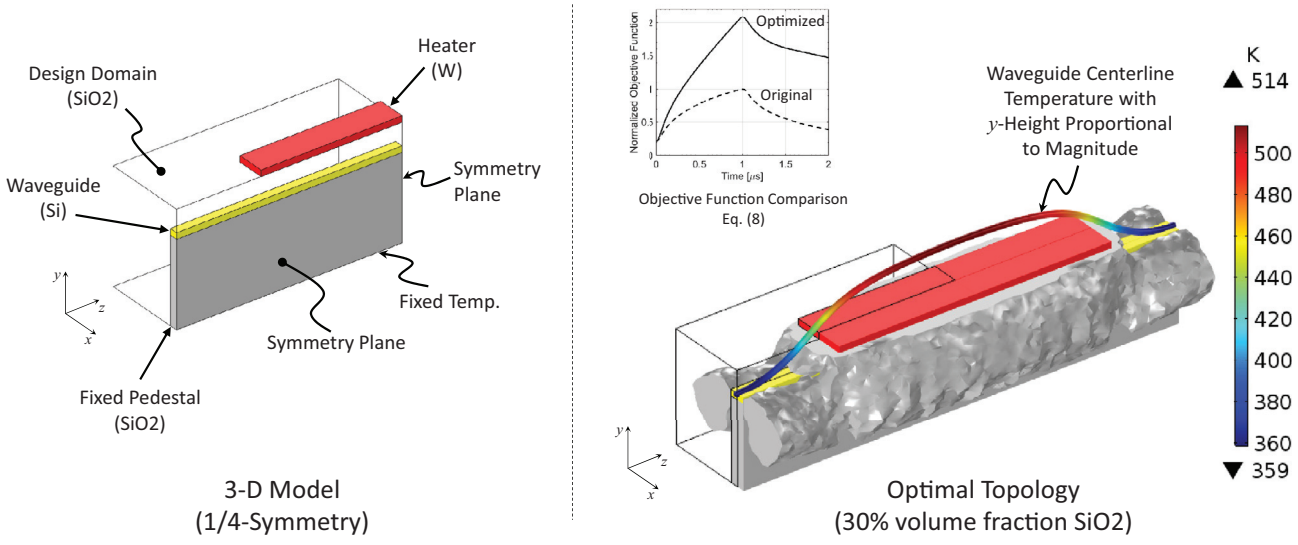

Fig. 12. 3-D optimization model (left) and optimization results for a SiO_2 volume fraction of 30% (right); note that the waveguide centerline temperature at $t = 0.5$ μs is superimposed on the optimization result as a line colored by temperature with y-direction height proportional to the magnitude, and the inset image shows the normalized objective function before and after optimization.

the ends of the optimized structure the SiO_2 material is removed from the top of the waveguide. This material removal, along with the termination of the over-clad heater, does induce roll-off in the waveguide temperature. Thus, the calculation of out-of-plane modulator length necessary to achieve a 2π phase shift, as described in Section 2.3, may be appropriately augmented by incorporating a sufficient end length to account for such temperature effects.

4. Conclusions

In this work, an optimization formulation relevant to the design of Si modulator opto-electronic devices was proposed. Using transient adjoint variables computed by a time reversal finite element procedure, the sensitivity of the objective function was obtained. An initial benchmark numerical example elucidated the effect of thermal capacitance on an optimal structural design confirming the expected behavior of the optimization approach. Additional studies of a Si modulator with an over-clad metal heater were then presented, and the design results highlighted faster modulator temperature rise time with reduced out-of-plane length based on a subsequent optical analysis. Future optimization formulations may include thermal cross-talk in the objective function formulation. Practical considerations including fabrication constraints, modulator reliability, and three-dimensional geometry effects should also be incorporated into any associated design process. Nonetheless, by exploiting the availability of efficient transient finite element analysis, transient sensitivity analysis, and topology optimization, we have developed and demonstrated a scheme to enhance the time-transient thermal response of compact Si modulator opto-electronic devices. The method is readily extendable to a range of more complex Si modulator designs involving multiple waveguides for next-generation sensors.

Declaration of Competing Interest

The authors declare that they have no known competing financial interests or personal relationships that could have appeared to influence the work reported in this paper.

CRediT authorship contribution statement

Gil Ho Yoon: Conceptualization, Methodology, Software, Investigation, Formal analysis, Writing - original draft, Writing - review & editing. **Ercan M. Dede:** Conceptualization, Methodology, Software, Investigation, Formal analysis, Writing - original draft, Writing - review & editing, Supervision. **Tsuyoshi Nomura:** Conceptualization, Methodology, Writing - review & editing. **Paul Schmalenberg:** Conceptualization, Methodology, Investigation, Formal analysis, Writing - review & editing.

References

[1] J. Song, J. Ding, Silicon Nanowire Waveguides and Their Applications in Planar Wavelength Division Multiplexers/demultiplexers, in: A. Hashim (Ed.), Nanowires, IntechOpen, Rijeka, 2011, pp. 1–24.

[2] P. Sun, R.M. Reano, Submilliwatt thermo-optic switches using free-standing silicon-on-insulator strip waveguides, Opt. Express 18 (8) (2010) 8406–8411.

[3] M.R. Watts, J. Sun, C. DeRose, D.C. Trotter, R.W. Young, G.N. Nielson, Adiabatic thermo-optic mach-zehnder switch, Opt. Lett. 38 (5) (2013) 733–735.

[4] C.-Y. Wu, P. Lin, R.-S. Huang, W.-C. Chao, M.M.H. Lee, Design optimization for micromachined low power mach-zehnder thermo-optic switch, Appl. Phys. Lett. 89 (12) (2006) 121121.

[5] X. Zhang, S. Chakravarty, C.-J. Chung, Z. Pan, H. Yan, R.T. Chen, Ultra-compact and wide-spectrum-range thermo-optic switch based on silicon coupled photonic crystal microcavities, Appl. Phys. Lett. 107 (22) (2015) 221104.

[6] Z. Lu, K. Murray, H. Jayatilleka, L. Chrostowski, Michelson interferometer thermo-optic switch on soi with a 50-w power consumption, IEEE Photon. Technol. Lett. 27 (22) (2015) 2319–2322.

[7] S. Lei, A. Shen, R. Enright, Thermo-optic tuning efficiency of micro ring resonators on low thermal resistance silicon photonics substrates, in: Proc. ASME 2017 International Technical Conference and Exhibition on Packaging and Integration of Electronic and Photonic Microsystems, San Francisco, California, Aug. 29-Sept. 1, 2017. V001T02A009

[8] M.P. Bendse, N. Kikuchi, Generating optimal topologies in structural design using a homogenization method, Comput. Method. Appl. Mech. Eng. 71 (2) (1988) 197–224.

[9] E.M. Dede, J. Lee, T. Nomura, Multiphysics Simulation - Electromechanical System Applications and Optimization, Springer-Verlag London, 2014.

[10] Y. Tsuji, K. Hirayama, T. Nomura, K. Sato, S. Nishiwaki, Design of optical circuit devices based on topology optimization, IEEE Photon. Technol. Lett. 18 (7) (2006) 850–852.

[11] J. Jensen, O. Sigmund, Topology optimization for nano-photonics, Laser Photon. Rev. 5 (2) (2011) 308–321.

[12] A.Y. Piggott, J. Lu, K.G. Lagoudakis, J. Petykiewicz, T.M. Babinec, J. Vučković, Inverse design and demonstration of a compact and broadband on-chip wavelength demultiplexer, Nat Photonics 9 (2015) 374.

[13] L. Su, R. Trivedi, N.V. Sapra, A.Y. Piggott, D. Vercruysse, J. Vučković, Fully-automated grating coupler design through adjoint optimization, in: Conference on Lasers and Electro-Optics, Optical Society of America, 2018, p. JW2A.60.

[14] J. Andkjær, S. Nishiwaki, T. Nomura, O. Sigmund, Topology optimization of grating couplers for the efficient excitation of surface plasmons, J. Opt. Soc. Am. B 27 (9) (2010) 1828–1832, doi:10.1364/JOSAB.27.001828.

[15] R.T. Haftka, Techniques for thermal sensitivity analysis, Int J Numer Methods Eng 17 (1) (1981) 71–80.

[16] R.A. Meric, Boundary elements for static optimal heating of solids, J Heat Transfer 106 (4) (1984) 876–880.

[17] C. Zhuang, Z. Xiong, A global heat compliance measure based topology optimization for the transient heat conduction problem, Numerical Heat Transfer, Part B: Fundamentals 65 (5) (2014) 445–471.

[18] Q. Li, G.P. Steven, O.M. Querin, Y. Xie, Shape and topology design for heat conduction by evolutionary structural optimization, Int J Heat Mass Transf 42 (17) (1999) 3361–3371.

[19] Q. Li, G.P. Steven, Y. Xie, O.M. Querin, Evolutionary topology optimization for temperature reduction of heat conducting fields, Int J Heat Mass Transf 47 (23) (2004) 5071–5083.

[20] Y.M.X. Qing Li Grant P. Steven, Thermoelastic topology optimization for problems with varying temperature fields, J. Therm. Stresses 24 (4) (2001) 347–366.

[21] S.-H. Ha, S. Cho, Topological shape optimization of heat conduction problems using level set approach, Numerical Heat Transfer, Part B: Fundamentals 48 (1) (2005) 67–88.

[22] S.-H. Ahn, S. Cho, Level set-based topological shape optimization of heat conduction problems considering design-dependent convection boundary, Numerical Heat Transfer, Part B: Fundamentals 58 (5) (2010) 304–322.

[23] K. Dems, B. Rousselet, Sensitivity analysis for transient heat conduction in a solid body – part i: external boundary modification, Structural Optimization 17 (1) (1999) 36–45.

[24] K. Dems, B. Rousselet, Sensitivity analysis for transient heat conduction in a solid body – part ii: interface modification, Structural Optimization 17 (1) (1999) 46–54.

[25] Z.-P. Wang, D. Kumar, On the numerical implementation of continuous adjoint sensitivity for transient heat conduction problems using an isogeometric approach, Struct. Multidiscip. Optim. 56 (2) (2017) 487–500.

[26] B.-S. Kang, G.-J. Park, J.S. Arora, A review of optimization of structures subjected to transient loads, Struct. Multidiscip. Optim. 31 (2) (2006) 81–95.

[27] R. Korycki, Sensitivity analysis and shape optimization for transient heat conduction with radiation, Int J Heat Mass Transf 49 (13) (2006) 2033–2043.

[28] S. Turteltaub, Optimal material properties for transient problems, Struct. Multidiscip. Optim. 22 (2) (2001) 157–166.

[29] Y. Gu, B. Chen, H. Zhang, R. Grandhi, A sensitivity analysis method for linear and nonlinear transient heat conduction with precise time integration, Struct. Multidiscip. Optim. 24 (1) (2002) 23–37.

[30] Y. Li, K. Saitou, N. Kikuchi, Topology optimization of thermally actuated compliant mechanisms considering time-transient effect, Finite Elem. Anal. Des. 40 (11) (2004) 1317–1331.

[31] C. Zhuang, Z. Xiong, H. Ding, Topology optimization of the transient heat conduction problem on a triangular mesh, Numerical Heat Transfer, Part B: Fundamentals 64 (3) (2013) 239–262.

[32] S. Wu, Y. Zhang, S. Liu, Topology optimization for minimizing the maximum temperature of transient heat conduction structure, Struct. Multidiscip. Optim. 60 (1) (2019) 69–82.

[33] G.H. Yoon, Topological design of heat dissipating structure with forced convective heat transfer, J. Mech. Sci. Technol. 24 (6) (2010) 1225–1233.

[34] E.M. Dede, Optimization and design of a multipass branching microchannel heat sink for electronics cooling, J. Electron. Packag. 134 (4) (2012) 041001–041001–10, doi:10.1115/1.4007159.

[35] J. Alexandersen, N. Aage, C.S. Andreasen, O. Sigmund, Topology optimisation for natural convection problems, Int. J. Numer. Method. Fluid. 76 (10) (2012) 699–721.

[36] D.A. Tortorelli, R.B. Haber, First-order design sensitivities for transient conduction problems by an adjoint method, Int. J. Numer. Method. Eng. 28 (4) (1989) 733–752.

[37] K. Chiang, Review of numerical and approximate methods for the modal analysis of general optical dielectric waveguides, Opt. Quantum Electron. 26 (3) (1994) S113–S134.
[38] K. Svanberg, The method of moving asymptotes – a new method for structural optimization, Int. J. Numer. Method. Eng. 24 (2) (1987) 359–373.
[39] COMSOL Multiphysics® v. 5.3, www.comsol.com. COMSOL AB, Stockholm, Sweden. 2017.
[40] A. Milenin, C. Jamois, T. Geppert, U. Gsele, R. Wehrspohn, SOI Planar photonic crystal fabrication: etching through SiO_2si/SiO_2 layer systems using fluorocarbon plasmas, Microelectron. Eng. 81 (1) (2005) 15–21.
[41] S. Chung, M. Nakai, H. Hashemi, Low-power thermo-optic silicon modulator for large-scale photonic integrated systems, Opt. Express 27 (9) (2019) 13430–13459.